Supplementary Information (SI) for Industrial Chemistry & Materials.

Supporting information

Imidazolium Ligand-Modified Cu_2O Catalysts for Enhancing C_{2+} Selectivity in CO_2 Electroreduction via Local *CO Enrichment

Rongzhen Chen,[a] Ling Zhang,[a] Yuhang Li*[a,b]

[a] Key Laboratory for Ultrafine Materials of Ministry of Education, Shanghai Engineering Research Center of Hierarchical Nanomaterials, School of Materials Science and Engineering, East China University of Science & Technology, Shanghai 200237, China

[b] Department of Chemical Engineering, School of Chemistry and Chemical Engineering, Shanghai Jiao Tong University, Shanghai 200240, China

Methods

Synthesis of electrocatalysts

(1) Cu_2O

First, 2.0 g of anhydrous sodium tetraborate ($Na_2B_4O_7$) was added to 70 mL of hot deionized water (90 °C) under continuous magnetic stirring for over 10 minutes to ensure complete dissolution, yielding a clear and homogeneous solution. After cooling the sodium tetraborate solution to room temperature, 0.8 g of sodium ascorbate was introduced into the mixture under vigorous stirring. The stirring was maintained for an additional 10 minutes, followed by the addition of 0.4 g of $CuCl_2$. Upon incorporation of $CuCl_2$, the solution immediately transitioned to an orange-yellow coloration. After 7 minutes of reaction, the resulting product was isolated via centrifugation, thoroughly washed with deionized water, and subsequently vacuum-dried at 60 °C for 12 hours.

(2) Cu_2O@Imidazole

Catalysts modified with imidazolium of varying alkyl chain lengths (C_2–C_{10}) were designated as EMIm-Cu_2O, PMIm-Cu_2O, BMIm-Cu_2O, HMIm-Cu_2O, OMIm-Cu_2O, and DMIm-Cu_2O, respectively. Take the synthesis of EMIm-Cu_2O as an example: First, 2.0 g of anhydrous sodium tetraborate ($Na_2B_4O_7$) was dissolved in 70 mL of hot deionized water (90 °C) under magnetic stirring for at least 10 minutes to form a clear solution. After cooling the solution to room temperature, 0.8 g of sodium ascorbate and 0.1 g of 1-ethyl-3-methylimidazolium tetrafluoroborate (EMImBF$_4$) were added sequentially to the sodium tetraborate solution under vigorous stirring. The mixture was stirred continuously for 10 minutes, followed by the addition of 0.4 g of $CuCl_2$. Upon introducing $CuCl_2$, the solution rapidly turned orange-yellow. After 7 minutes, the product was collected via centrifugation, washed repeatedly with deionized water, and vacuum-dried at 60 °C for 12 hours. The synthesis procedures for PMIm-Cu_2O, BMIm-Cu_2O, HMIm-Cu_2O, OMIm-Cu_2O, and DMIm-Cu_2O were identical to that of EMIm-Cu_2O, except that EMImBF$_4$ was replaced with the corresponding imidazolium salts: PMImBF$_4$ (1-propyl-3-methylimidazolium tetrafluoroborate), BMImBF$_4$ (1-butyl-3-methylimidazolium tetrafluoroborate), HMImBF$_4$ (1-hexyl-3-methylimidazolium tetrafluoroborate), $OMImBF_4$ (1-octyl-3-methylimidazolium tetrafluoroborate), $DMImBF_4$ (1-decyl-3-methylimidazolium tetrafluoroborate).

Catalysts characterization

We detected the morphology and elemental distributions of the catalysts by transmission electron microscope (JEM-2100) and energy dispersive X-ray spectroscopy (Talos F200). We verified the crystal structures by a X-ray diffractometer (Bruker D8). We performed ATR-Fourier transform infrared spectroscopy by a Nicolet 6700 FTIR spectrometer. We confirmed the valence states by X-ray photoelectron spectroscopy (ESCALAB 250Xi).

CO_2 electroreduction tests

Electrochemical measurements were conducted using an electrochemical workstation (CHI 760E). Catalysts were loaded on the gas diffusion electrodes (GDL, 2×2 cm^2) as working electrodes. For flow cell, the tests were carried out in a home-made flow cell reactor. Ag/AgCl (KCl-saturated) and nickel foam were reference electrode and counter electrode, respectively. CO_2 gas was flowed into the catholyte in gas chamber of flow cell with a rate of 25 sccm. In flow cell, the electrolyte was pumped and circulated (10 ml/min). For the gas products analysis, we used an online gas chromatography (GC2060) with flame ionization detector (FID) and thermal conductivity detector (TCD). To measure the liquid products, we used nuclear magnetic resonance spectrometry (Agilent DD2 600 MHz). The catalysts were tested at each current density for 30 min using chronopotentiometry method with three times GC sampling. After tested at each current density, the electrolyte was collected to detect the liquid products. Electrode potentials were converted to the RHE scale using E (versus RHE) = E (Ag/AgCl, saturated KCl) + 1.031. Linear sweep voltammetry was performed at a scan rate of 50 mV s^{-1}. The faradaic efficiencies (FE) of the products were calculated using equation (1):

$$\text{Faradaic Efficiency (\%)} = 100 \times \frac{nFc}{Q} \qquad (1)$$

where *n* is the number of electrons used in producing the products from CO_2, F is the Faradaic constant (96485 C mol^{-1}), c is the amount of the product (mol), and Q is the total charge for the reduction process.

The double-layer capacitance (C_{dl}) of the catalysts was estimated by measuring the capacitive current density associated with different scan rates via cyclic voltammetry (CV) curves in a non-faradaic region in CO_2-flowed 1 M KOH. The scan rates were 10, 20, 30, 40, 50, and 60 mV s^{-1}, respectively. By plotting the $\Delta J = (Ja - Jc)$ at middle potential against the scan rate (where Ja and Jc are the anodic and cathodic current density, respectively), the C_{dl} was determined to be half that of the linear fitting slope.

In Situ ATR-SEIRAS

A polycrystalline Au nanofilm was deposited chemically onto a Si ATR-IR prism. The Si prism was first polished using a 0.05 μm alumina solution until the reflecting surface becomes hydrophobic. The alumina powder was then washed off the surface of the crystal by sonicating in alternate baths of water, acetone, and water. Further, the cleaned crystal face was immersed in a 40% NH_4F bath for 5 minutes to remove the native oxide layer and create a hydride-terminated surface. The reflecting surface was then immersed in a plating solution by a mixture of 3 mL 5 wt.% HF and a gold plating solution consisting of $NaAuCl_4\cdot 2H_2O$ (0.009 M), NH_4Cl (0.03 M), Na_2SO_3 (0.09 M), $Na_2S_2O_3\cdot 5H_2O$ (0.03 M) and NaOH (0.03 M) at 55 °C for 5 min to deposit the Au film. Then, catalysts were coated onto Au nanofilm as the working electrode. A platinum wire and Ag/AgCl (saturated KCl) were used for the counter and reference electrodes, respectively. A single compartment electrochemistry cell was used to test. ATR-SEIRAS experiments were conducted with Perkin Elmer Spectrum 100 FT-IR spectrometer equipped with a liquid nitrogen-cooled MCT detector and a Si attenuated total reflection (UATR) accessory. The spectral resolution was set to 4 cm^{-1}. The data were collected with ~40 s resolution per spectrum and measured simultaneously by the chronoamperometry technique between open circuit potential (~ 0.1 V) to -1.6 V. Before the spectra were collected, the work electrodes were pre-reduced by cyclic voltammetry (0.2 V to -1.2 V, 50 mV s^{-1}, 20 cycles) to keep the catalyst in a relatively stable state.

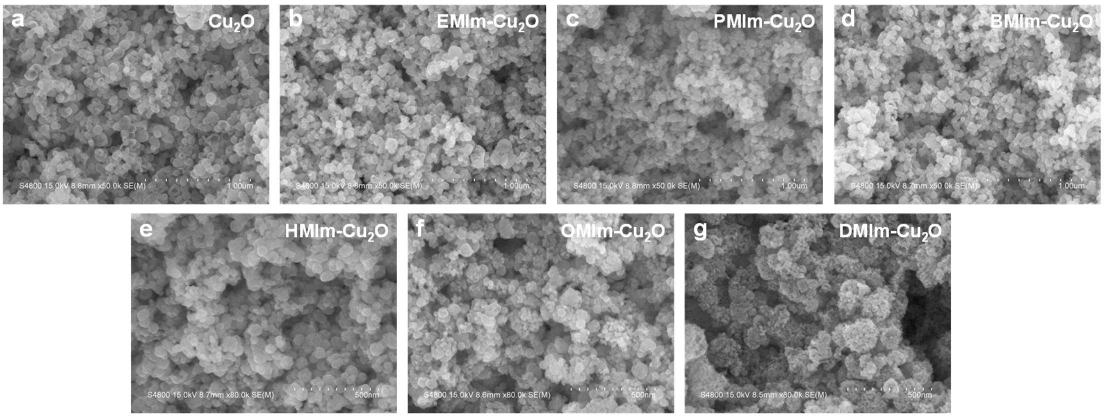

Fig. S1. SEM images of Cu_2O@Imidazole catalysts. a) Cu_2O, b) EMIm-Cu_2O, c) PMIm-Cu_2O, d) BMIm-Cu_2O, e) HMIm-Cu_2O, f) OMIm-Cu_2O, g) DMIm-Cu_2O.

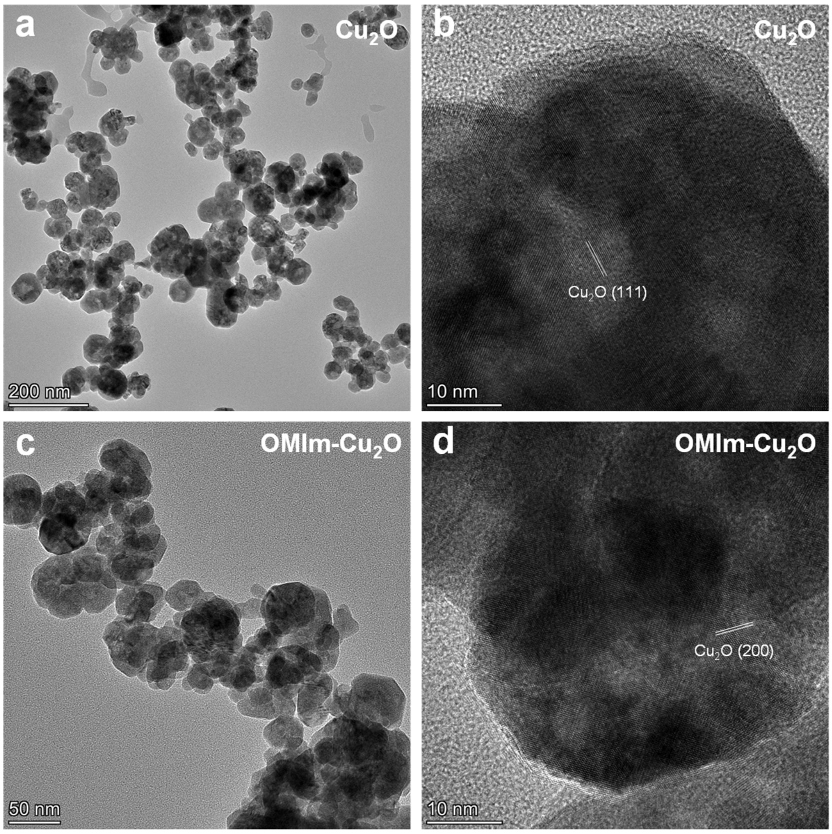

Fig. S2. a~b) TEM images of Cu_2O. c~d) TEM images of OMIm-Cu_2O.

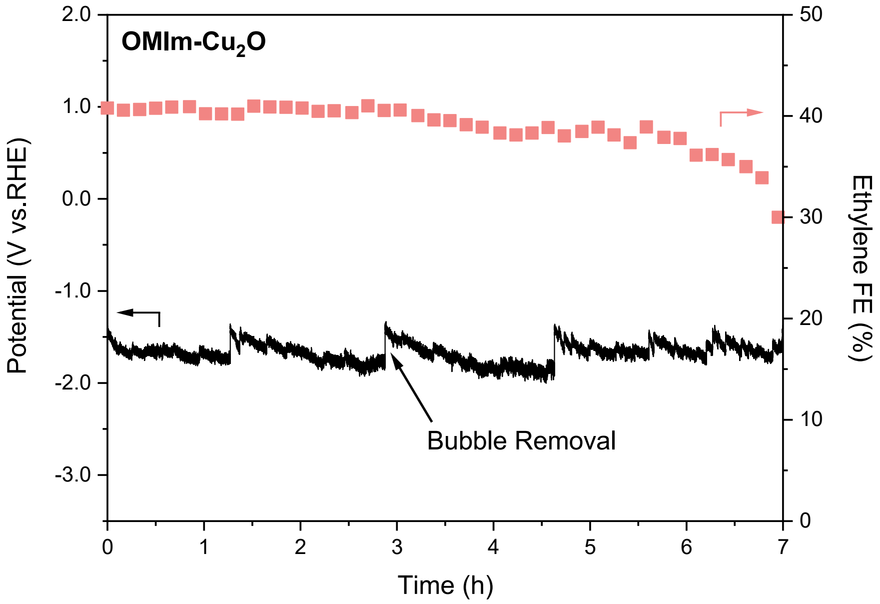

Fig. S3. Stability voltage-time curve of OMIm-Cu$_2$O in CO$_2$RR and its C$_2$H$_4$ selectivity.

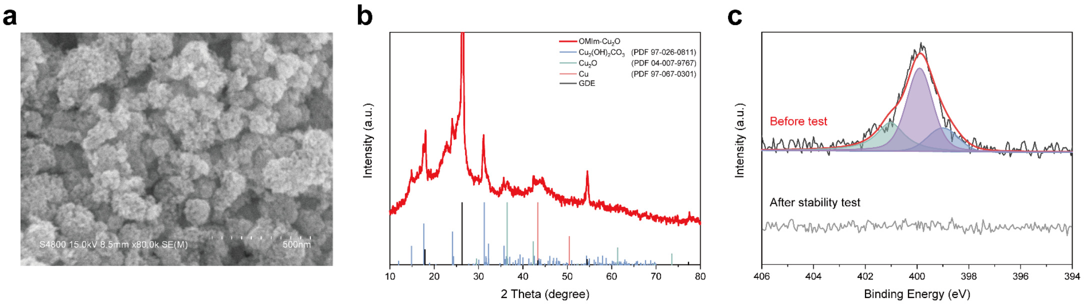

Fig. S4. a) SEM image of OMIm-Cu$_2$O after the stability test. b) XRD pattern of OMIm-Cu$_2$O after the stability test. c) Comparison of N 1s XPS spectra of OMIm-Cu$_2$O before and after the reaction.

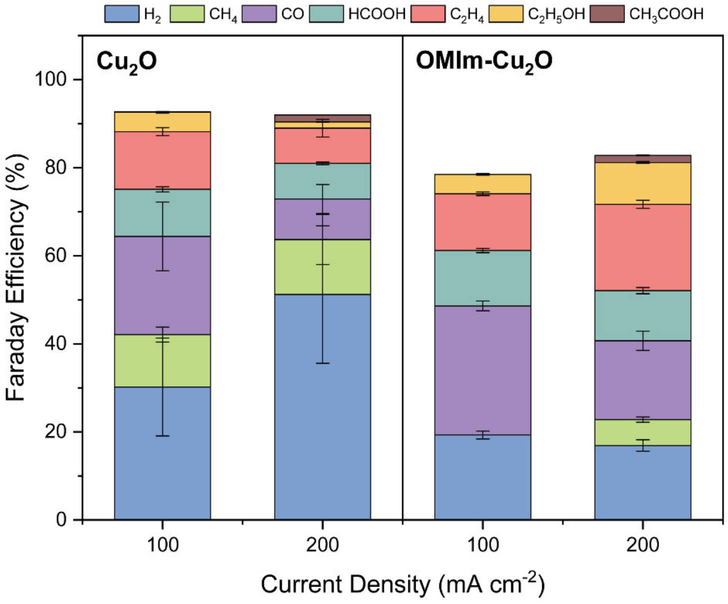

Fig. S5 Product FE of Cu$_2$O and OMIm-Cu$_2$O at different applied current densities under acidic conditions.

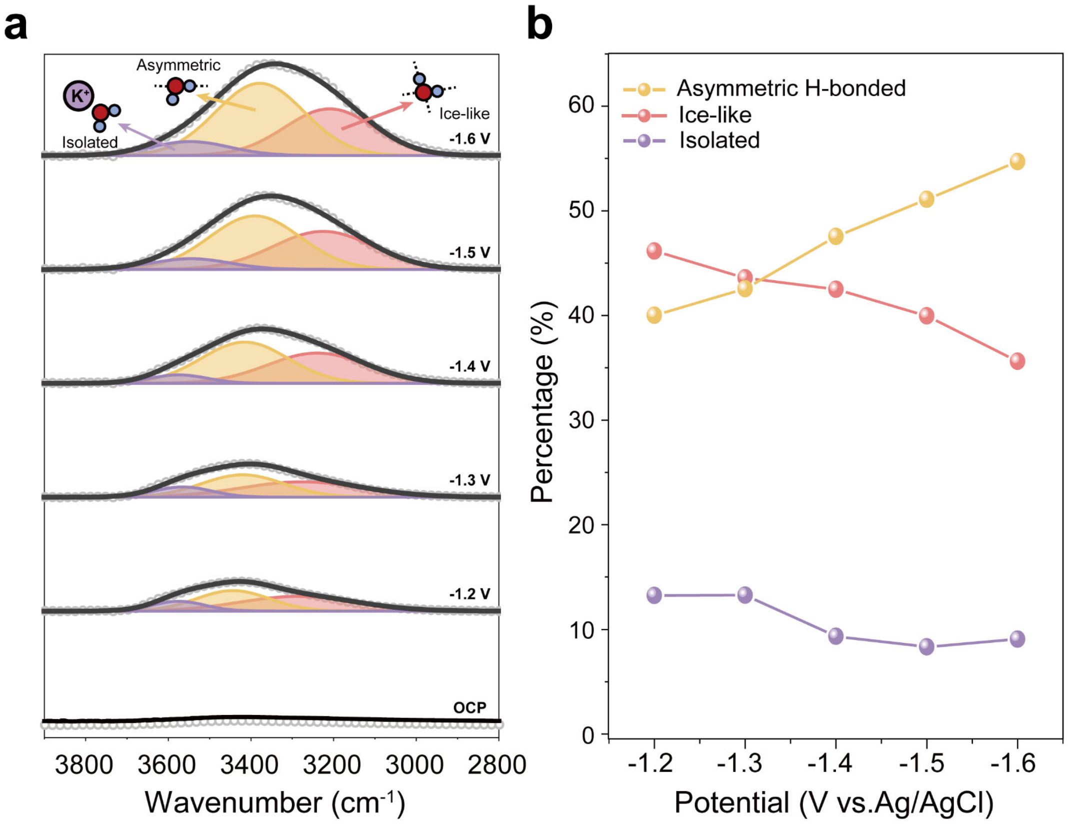

Fig. S6 a) In situ ATR-SEIRAS spectra of interfacial H_2O during CO_2RR on a BMIm-Cu_2O electrode in 1 M $KHCO_3$. b) The ratio of the three water peaks at the BMIm-Cu_2O interface during CO_2RR, obtained from the peak area ratio after Gaussian fitting.

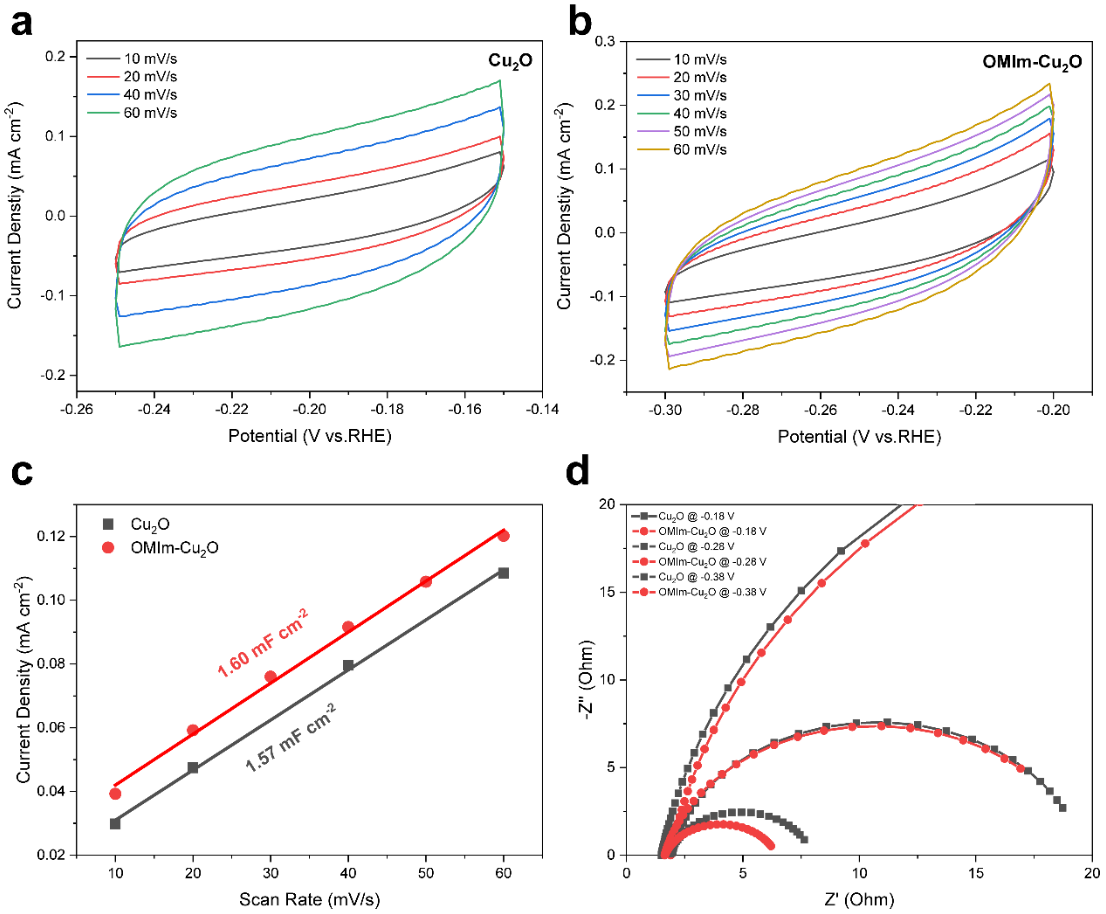

Fig. S7 a) Cyclic voltammetry curves of Cu_2O and b) OMIm-Cu_2O at different scan rates. c) Linear relationship between the double layer current and scan rate of Cu_2O and OMIm-Cu_2O to estimate ECSA. d) Impedance spectra of Cu_2O and OMIm-Cu_2O tested at -0.18, -0.28 and -0.38 V vs. RHE.

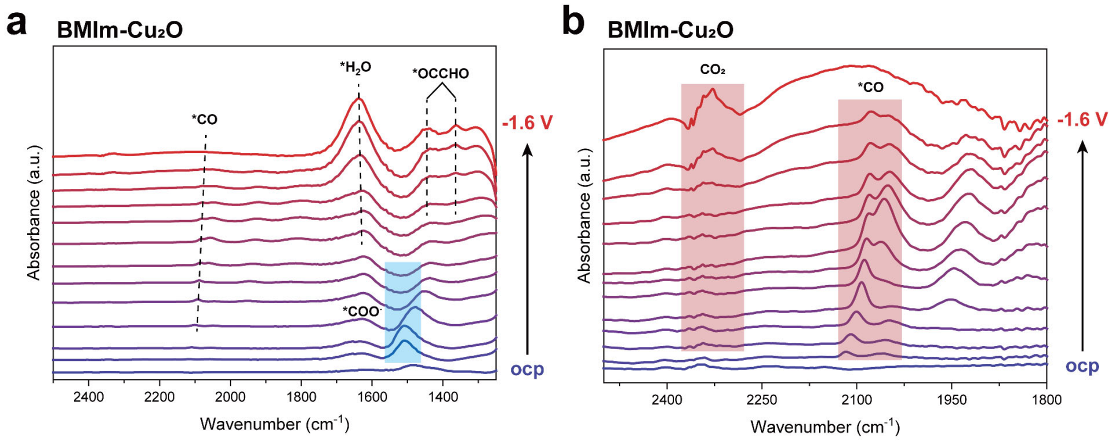

Fig. S8 a) In situ ATR-SEIRAS spectra of BMIm-Cu_2O in CO_2-saturated 1 M $KHCO_3$ electrolyte. b) Magnified in situ ATR-SEIRAS spectra of BMIm-Cu_2O in the range of 2500~1800 cm^{-1}.

Table S1. Performance Comparison with Literature-Reported Surface-Modified Imidazolium-Based Ligand Catalysts

Catalyst	**Ligand**	**Eletrolyte**	**Electrolyzer**	**Main Product**	**FE**	**Partial Current Density**	**Reference**
BMIm-Cu_2O	1-butyl-3-methylimidazolium	1 M KOH	Flow cell	CO	64.6	129.2	this work
BMIm-Cu_2O	1-butyl-3-methylimidazolium	3 M KCl	Flow cell	CO	51.1	51.3	this work
OMIm-Cu_2O	1-octyl-3-methylimidazolium	1 M KOH	Flow cell	C_2	63.3	504	this work
OMIm-Cu_2O	1-octyl-3-methylimidazolium	3 M KCl	Flow cell	C_2	30.7	61.4	this work
Cu@AIL	1-aminopropyl-3-methylimidazolium	1 M KOH	Flow cell	C_2	71.6	1288.8	J. Am. Chem. Soc. 2023, 145, 21983−21990
IL@Cu	1-butyl-3-methylimidazolium	0.1 M KHCO3	H cell	C_2H_4	77.3	26.4	Angew. Chem. Int. Ed. 2022, 61, e202200039
Cu Foam-IL	1-butyl-3-methylimidazolium	0.1 M KHCO3	H cell	CO	15	<1	Angew. Chem. Int. Ed. 2020, 59, 18095 – 18102
CuNP-EMIM	1-ethyl-3-methylimidazolium	3 M KCl	Flow cell	C_2	60	180	Chem. Mater. 2023, 35, 7060−7068
[EMIM][BF_4]@$Cu_3(BTC)_2$	1-ethyl-3-methylimidazole	0.5 M KHCO3	Flow cell	C_2H_4	44	~60	Chem. Eng. J., 2025, 513, 162872
planar Cu foils	1-butyl-3-(1,10-phenanthrolin-2-yl)-imidazolium	0.1 M KHCO3	H cell	C_2H_4	73	<1	ACS Appl. Mater. Interfaces 2022, 14, 24, 27823–27832